Article

Not peer-reviewed version

MR protocol optimization for Hepatobiliary Phase Imaging with Gadoxetic Acid for 1.5T: Comparison Between Breath-Hold T1-weighted and High Resolution Navigated 3D T1-weighted sequences

Eliseo Picchi , Valentina Ferrazzoli , Valeria Liberto , Luca Toti , Raffaella Giocondo , Valerio Da Ros , Noemi Pucci , Silvia Minosse , Francesco Garaci , Francesca Di Giuliano *

Posted Date: 17 June 2024

doi: 10.20944/preprints202406.1104.v1

Keywords: Magnetic Resonance; Gadoxetic Acid; High Resolution Navigated 3D; Hepatocarcinoma

Article

MR Protocol Optimization for Hepatobiliary Phase Imaging with Gd-EOB-DTPA for 1.5T: Comparison between Breath-Hold T1-Weighted and High Resolution Navigated 3D T1-Weighted Sequences

Eliseo Picchi [1,†], Valentina Ferrazzoli [2,†], Valeria Liberto [1], Luca Toti [3], Raffaella Giocondo [1], Valerio Da Ros [1], Noemi Pucci [1], Silvia Minosse [1], Francesco Garaci [2] and Francesca Di Giuliano [2,*]

[1] Diagnostic Imaging Unit, Department of Biomedicine and Prevention, University of Rome Tor Vergata, Viale Oxford 81, 00133, Rome, Italy. eliseo.picchi@hotmail.it ; valelib84@gmail.com; raffaellagiocondo@gmail.com; darosvalerio@gmail.com; puccinoemi@gmail.com; silviaminosse2@gmail.com

[2] Neuroradiology Unit, Department of Biomedicine and Prevention, University of Rome Tor Vergata, Viale Oxford 81, 00133, Rome, Italy. valentinaferrazzoli@hotmail.it; garaci@gmail.com; francescadigiuliano@msn.com

[3] HPB and Transplant Unit, Department of Surgical Sciences, University of Rome Tor Vergata, Rome, Italy lucatoti@gmail.com

* Correspondence: francescadigiuliano@msn.com; Tel.: +0039-0620902400-01

† These authors contributed equally to this work.

Abstract: Background and Objectives: This study aims to compare the efficacy of navigator-gated three-dimensional T1-weighted gradient-echo sequences (NAV) with standard breath-hold T1-weighted gradient-echo sequences (BH) in detecting Hepatocellular carcinoma (HCC) nodules in patients with chronic viral hepatitis undergoing magnetic resonance imaging (MRI) with Gadolinium ethoxybenzyl-diethylenetriaminepentaacetic acid (Gd-EOB-DTPA). **Methods and materials:** From May 2022 until November 2023, 58 Fifty-eight patients from the HPB and Transplant Unit at the University Hospital "Policlinico Tor Vergata" in Rome, Italy, were included in the retrospective study . Eligible patients had chronic viral hepatitis and at least one hepatic nodule of one cm or larger detected by ultrasound. Each patients underwent an MRI that included NAV and BH sequences using various flip angles (FA) ranging from 10° to 40° post Gd-EOB-DTPA administration. Three independent radiologists conducted qualitative analysis (Clearness of the image, Presence and type of artifacts and Diagnostic reliability) of the sequences, and the contrast-to-noise ratio (CNR) between lesions and healthy liver, as well as between liver and spleen, was evaluated. **Results:** NAV sequences at a FA of 40°, demonstrated the highest agreement across all quality parameters ($p<0,001$). A comparison of CNR between hypointense lesions and healthy liver tissue showed decreasing values with increase FA, notably in NAV sequences. Statistically significant differences were observed among the sequences: BH 10° 0.73±0.17; BH 30° 0.68±0.17; BH 40° 0.68±0.15; NAV 25° 0.62±0.18; NAV 40° 0.56±0.17. In contrast comparisons between liver and spleen, the trend indicated an increase in CNR and contrast in sequences with higher FA, with the differences between BH and NAV at 40° FA not being statistically significant. **Conclusion**: The study emphasizes the diagnostic superiority of NAV over BH sequences with a 40° FA in assessing image quality and enhancement in malignant liver nodules of cirrhotic patients. Incorporating one of these sequences into MRI protocols is recommended for enhanced diagnostic clarity, which is critical for informed surgical planning. This could facilitate more precise interventions, potentially improving surgical outcomes in the management of hepatocellular carcinoma.

Keywords: magnetic resonance; Gadoxetic acid; high resolution navigated 3D; hepatocarcinoma

 doi:10.20944/preprints202406.1104.v1

Introduction

Hepatocellular carcinoma (HCC) ranks as the fifth most common cancer globally, with an annual incidence estimated at 500.000 cases [1] . The diagnosis and staging of HCC are primarily conducted using contrast-enhanced computed tomography (CECT) and dynamic contrast-enhanced magnetic resonance (DCE-MRI), as outlined in the latest clinical practice guidelines by the European Association for the Study of the Liver, the European Organisation for Research and Treatment of Cancer (EASL-EORTC), and the American Association for the Study of Liver Diseases (AASLD) [2–4].

Although not mandatory in the international guidelines on HCC management, magnetic resonance imaging (MRI) with hepatospecific contrast agents has demonstrated higher sensibility and specificity for the non-invasive detection of HCC nodules compared to contrast-enhanced ultrasound (CEUS) and CECT [2,4,5]. Moreover, the 2021 Consensus report from the 10th International Forum for Liver Magnetic Resonance Imaging and earlier the recommendations from the Japan Society of Hepatology have recognized hepatobiliary-enhanced MRI as a precise method for diagnosing and staging HCC[6].

MRI has shown superior performance over CT in detecting small lesions, although its sensitivity remains relatively low at 62% for nodules smaller than 20 mm. Enhancing the diagnostic accuracy of MRI with Gadolinium ethoxybenzyl-diethylenetriaminepentaacetic acid (Gd-EOB-DTPA) hinges on using specific sequences during the hepatobiliary phase (HBP), which are critical for improving lesion detection.

Despite its advantages, the ideal flip angle (FA) for detecting HCC nodules using this method remains unclear, with ongoing debates and conflicting findings in the current literature [7–11].

This study aims to optimize the hepatobiliary MRI scanning protocol using Gd-EOB-DTPA. It compares T1-weighted breath-hold (BH) sequences and free-breathing (or rather triggered) sequences with different flip angles (FA) from 10° to 40° with high resolution NAV to identify HCC nodules, based on both qualitative and quantitative analyses.

Accurate imaging is imperative not only for diagnosis but also for surgical planning. Enhancing the resolution and accuracy of hepatobiliary phase imaging directly impacts the surgical approach to liver resection and transplantation. Techniques in recipient hepatectomy have evolved to improve oncological outcomes in liver transplantation for hepatocellular carcinoma, underscoring the necessity for precise preoperative imaging to guide surgical decisions[12].

Furthermore, the risk of de novo malignancies post-transplant emphasizes the need for meticulous surgical planning and follow-up, which begins with reliable imaging [13]. The role of advanced imaging modalities, such as contrast-enhanced intraoperative ultrasound, highlights the continual integration of dynamic imaging technologies to improve detection and management of liver lesions during surgeries [5].

Materials and Methods

Patients

From May 2022 until November 2023, Fifty-eight patients from the HPB and Transplant Unit at the University Hospital “Policlinico Tor Vergata” in Rome, Italy, were included in the retrospective study. The inclusion criteria for patients were chronic viral hepatitis and at least one hepatic nodule of one centimeter or greater in diameter, detected by ultrasound in a surveillance program. Exclusion criteria included a glomerular filtration rate < 30 mL/min and total bilirubin levels exceeding 1.2 mg/dL.

All patients underwent MRI with hepatospecific Gd-EOB-DTPA contrast medium (0,1 mmol/ml) and provided informed consent in accordance with the Declaration of Helsinki.

The images were archived in the RIS-PACS system for re-evaluation.

 doi:10.20944/preprints202406.1104.v1

Examination Technique

The examinations were conducted using a high-field Achieva 1.5T scanner (Philips Medical Systems TM, Best, The Netherlands) with a 16-channel surface coil. Patients were positioned supine and fasted for at least four hours prior to the scanning. The MRI protocol began with the acquisition of axial T1-weighted gradient-echo (GRE) sequences in both in-phase and out-of-phase, as well as coronal Half-Fourier Acquisition Single-Shot Turbo-Spin Echo (HASTE) sequences.

Contrast administration involved 0.1 mol/ml Gd-EOB-DTPA at a dosage of 1mL per 10 kg body weight, delivered at a flow rate of 2 mL/s, followed by a 20 mL saline bolus at a flow rate of 3 mL/s. T1-weighted spoiled gradient-echo (SPGR) fat-sat volumetric sequences were then captured during the early arterial (15 seconds), late arterial (35 seconds), portal venous (70 seconds), and equilibrium phases (150 seconds). Additional imaging included T2-weighted Turbo-Spin Echo (TSE) sequences, Spectral Adiabatic Inversion Recovery (SPAIR) sequences, and diffusion-weighted imaging on the axial plane. During the hepatobiliary phase (HBP), occurring between 15 and 25 minutes post-Gd-EOB-DTPA administration, sequences were acquired as detailed in Table 1.

Table 1. MRI acquisition protocol during hepatobiliary phase following Gd-EOB-DTPA administration.

PARAMETERS	T1-weighted SPGR volumetric fat-sat BH	T1-weighted SPGR volumetric fat-sat BH	T1-weighted SPGR volumetric fat-sat BH	T1-weighted SPGR NAV free-breathing	T1-weighted SPGR NAV free-breathing
TR/TE (ms)	3.6/9.1	6.50/3.3	8.00/4.2	10/4.6	10/4.6
MATRIX	180x154	180x154	180x154	224 x121	224 x121
Reconstruction Voxel (mm)	0.71x0.71x2.60	0.71x0.71x2.60	0.71x0.71x2.60	0.98 x 0.98 x 2.50	0.98 x 0.98 x 2.50
AVERAGE DURATION (sec)	16	20	24	200	200
FLIP ANGLE (°)	10	30	40	25	40

Imaging Analysis

The quality and enhancement of images acquired from the three T1-weighted BH sequences with FA of 10°, 30°, 40° as well as the NAV ones with FA of 25° and 40°, were rigorously evaluated. Image quality was subjectively assessed using the following parameters:

- Clearness of the image: definition of the edges of examined structures was scored on a scale from 1 to 5, where 1 represents poor clearness, 2 is sub-optimal, 3 sufficient, 4 good, 5 optimal.
- Presence and type of artifacts: this included respiratory ghosting, aliasing, zebra artifacts, and pixel granularity, scored from 1 to 4, where 1 indicates severe (not diagnostic images), 2 moderate (modest effects on diagnosis), 3 unsubstantial (no effects on diagnosis) and 4 absent).
- Diagnostic reliability: the radiologist's confidence in lesion detection was scored from 1 to 5 where 1 denotes poor (impossible diagnosis), 2 sub-optimal (suspected diagnosis), 3 sufficient (possible diagnosis), 4 good (probable diagnosis), and 5 optimal (definitive diagnosis).

Three regions of interest (ROIs), each approximately 9 mm^2, were placed in areas of homogeneous signal intensity (SI) within hypointense focal lesions and in hepatic and splenic parenchyma. The contrast-to-noise ratio (CNR) was calculated by the formula:

$$CNR_{\text{lesion-liver}} = (SI_{\text{HCC}} - SI_{\text{liver parenchyma}}) / SD_{\text{image noise}}$$

$$CNR_{\text{liver-spleen}} = (SI_{\text{liver parenchyma}} - SI_{\text{splenic parenchyma}}) / SD_{\text{image noise}}$$

There measures served as the absolute parameters for comparing the different sequences analysed.

The evaluation was conducted independently by three radiologists with 10, 8 and 4 years of experience in body MRI analysis, who were blinded to the patient's clinical histories.

 doi:10.20944/preprints202406.1104.v1

Statistical Analysis

Interobserver agreement regarding the clearness of images, presence of artifacts, and diagnostic reliability was evaluated using the intraclass correlation coefficient (ICC). The ICC values were classified as follows:

- slight agreement: ICC <0.2
- fair agreement: ICC 0.2–0.4
- moderate agreement: ICC 0.4–0.6
- good agreement: ICC 0.6-0.8
- excellent agreement ICC > 0.8

Agreement levels were determined separately for each imaging sequence (BH 10°, BH 30°, BH 40°, NAV 25°, NAV 40°).

The results from each one of the three radiologists were compiled, presenting the mean values along with standard deviations. The Wilcoxon non-parametric statistical test was employed to compare each pair of sequences. A p-value of less than 0,05 was considered statistically significant.

Results

Evaluation of Image Quality

Image quality scores assigned by reader 1, reader 2 and reader 3 for both BH and NAV sequences are documented in Supplementary Tables 1, 2 and 3. Interobserver agreement for image quality parameters ranged from good to excellent. Notably, the BH sequences with a FA of 40° exhibited the lowest level of consensus in contrast, the NAV sequences with a 40° flip angle, demonstrated the highest interobserver agreement across all quality parameters. The ICC for the NAV sequences were as follows: for clearness, 0.93; for artifacts, 0.71; and for diagnostic reliability respectively 0.79 **(**as shown in Table 2).

Table 2. Intraclass correlation coefficient (ICC) statistics results.

	ICC - (p value)		
	CLEARNESS	**ARTIFACTS**	**DIAGNOSTIC RELIABILITY**
BH 10°	0.66 (0.001)	0.62 (0.001)	0.60 (0.001)
BH 30°	0.66 (0.001)	0.64 (0.001)	0.65 (0.001)
BH 40°	0.65 (0.001)	0.40 (0.004)	0.20 (0.020)
NAV 25°	0.79 (0.001)	0.39 (0.031)	0.68 (0.001)
NAV 40°	0.93 (0.001)	0.71 (0.001)	0.79 (0.001)

P-value is reported for each parameter (clearness of the image, artifacts and diagnostic reliability) by comparing scores given by observers. *P*-value <0.05 was considered statistically significant. Almost all the values have reported a statistically significant *p*-value.

Table 3. Summary statistics for the parameters n°1 (clearness), n°2 (artifacts), and n°3(diagnostic reliability). Data are expressed as mean and range.

	CLEARNESS OF THE IMAGE	**ARTIFACTS**	**DIAGNOSTIC RELIABILITY**
BH 10°	4.23 ± 0.44	3.70 ± 0.37	4.29 ± 0.43
BH 30°	3.83 ± 0.38	3.26 ± 0.42	4.03 ± 0.47
BH 40°	3.09 ± 0.39	2.76 ± 0.29	3.20 ± 0.33
NAV 25°	4.23 ± 0.48	3.37 ± 0.36	4.24 ± 0.48
NAV 40°	4.62 ± 0.52	3.76 ± 0.35	4.77 ± 0.38

Parameter n°1 (clearness of the image)

All sequences demonstrated good level of image clearness with average score > 4, as detailed in Table 3. However, the BH sequence at a 40° FA was an exception, recording a lower average score

 doi:10.20944/preprints202406.1104.v1

of 3.09±0.39. NAV sequences obtained better results for this parameter compared to the BH sequences, as shown in Table 4.

Table 4. Wilcoxon test results.

CLEARNESS OF THE IMAGE		ARTIFACTS		DIAGNOSTIC RELIABILITY	
SEQ	**P-VALUE**	**SEQ**	**P-VALUE**	**SEQ**	**P-VALUE**
BH 10° > BH 30°	< 0.0001	BH 10° > BH 30°	< 0.0001	BH 10° > BH 30°	< 0.0001
BH 10° > BH 40°	< 0.0001	BH 10° > BH 40°	< 0.0001	BH 10° > BH 40°	< 0.0001
NAV 25° > BH 10°	0.92	BH 10° > NAV 25°	< 0.0001	BH 10° > NAV 25°	0.19
NAV 40° > BH 10°	< 0.0001	NAV 40° > BH 10°	0.09	NAV 40° > BH 10°	< 0.0001
BH 30° > BH 40°	< 0.0001	BH 30° > BH 40°	< 0.0001	BH 30° > BH 40°	< 0.0001
NAV 25° > BH 40°	< 0.0001	NAV 25° > BH 40°	< 0.0001	NAV 25° > BH 40°	< 0.0001
NAV 40° > BH 40°	< 0.0001	NAV 40° > BH 40°	< 0.0001	NAV 40° > BH 40°	< 0.0001
NAV 40° > NAV 25°	< 0.0001	NAV 40° > NAV 25°	< 0.0001	NAV 40° > NAV 25°	< 0.0001

P-value for each parameter (clearness of the image, artifacts and diagnostic reliability) by comparing MRI sequences. *P*-value <0.05 was considered statistically significant. Almost all the values have reported a statistically significant *p*-value.

Parameter n°2 (artifacts evaluation)

Artifacts were generally minimal or absent across all sequences, with average scores > 3 (Table 3). The sequences most affected by evident artifacts were the BH 30° and BH 40°. This is likely due to the longer apnoea required during acquisition, which may have contributed to increased movement artifacts. Statistical analysis confirmed significant differences among the sequences, as indicated in Table 4.

Parameter n°3 (diagnostic reliability)

Diagnostic reliability was generally rated as good across all sequences. However, the BH sequence with FA of 40° was an exception, achieving only a barely sufficient rating, as noted in Table 3.. Statistically significant differences were observed among all sequences, underscoring the variance in diagnostic confidence provided by each, as detailed in Table 4.

Relative Enhancement Evaluation

Parameter n°1 (comparison Contrast-to-Noise Ratio (CNR) between lesions and healthy liver)

The CNR comparison between hypointense lesions and healthy liver tissue indicated progressively decreasing values, with increase of contrast enhancement, related to the augmentation of FA and in NAV sequences with average scores: BH 10° 0.73±0.17; BH 30° 0.68±0.17; BH 40° 0.68±0.15; NAV 25° 0.62±0.18; NAV 40° 0.56±0.17. Statistically significant differences resulted among the sequences (Table 5).

Table 5. Wilcoxon test results.

CNR LESION/LIVER	
SEQ	**P-VALUE**
BH 10° > BH 30°	0.0002
BH 10° > BH 40°	0.005
BH 10° > NAV 25°	0.0001
BH 10° > NAV 40°	0.0001
BH 30° > BH 40°	0.31
BH 40° > NAV 25°	0.0002
BH 40° > NAV 40°	0.0001
NAV 25° > NAV 40°	0.0001
CNR LIVER/SPLEEN	
SEQ	**P-VALUE**
BH 30° > BH 10°	0.0001
BH 40° > BH 10°	0.0001

 doi:10.20944/preprints202406.1104.v1

NAV 25° > BH 10°	0.0001
NAV 40° > BH 10°	0.0001
BH 40° > BH 30°	0.0001
NAV 25° > BH 40°	0.12
NAV 40° > BH 40°	0.21
NAV 40° >NAV 25°	0.86

We reported *p*-value of the contrast-to noise ratio (CNR) between lesions/liver and liver/spleen for each comparison between MRI sequences. *P*-value <0.05 was considered statistically significant. Almost all the values have reported a statistically significant *p*-value.

Parameter n°2 (CNR between liver and spleen)

The analysis of CNR between liver and spleen revealed an overall increase in CNR and contrast enhancement in sequences with higher FA and NAV. The average CNR scores were as follows:

- BH 10°: 1.58±0.52
- BH 30°: 2.23±0.82
- BH 40°: 2.47±0.84
- NAV 25°: 2.6±0.93
- NAV 40°: 2.62±0.86

The comparative analysis indicated that the differences between the BH sequences with an FA of 40° and NAV sequences were not statistically significant, as documented in Table 5.

Figures 1 and 2 display representative cases to visually illustrate these findings, providing a clear view of how different MRI sequences affect the CNR between liver and spleen tissues.

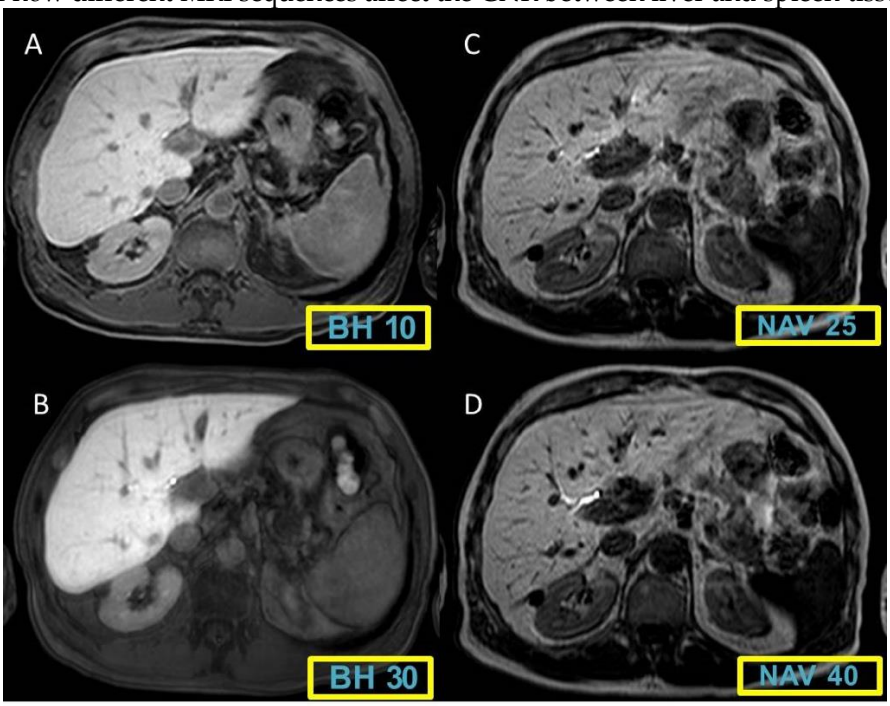

Figure 1. Breath-hold (BH) sequences (flip angle 10° and 30°) (A-B) and free-breathing navigated sequences (NAV) with flip angle of 25° and 40° (C-D). Free-breathing navigated sequences show a better enhancement with a higher image contrast compared to Breath-hold (BH) sequences.

 doi:10.20944/preprints202406.1104.v1

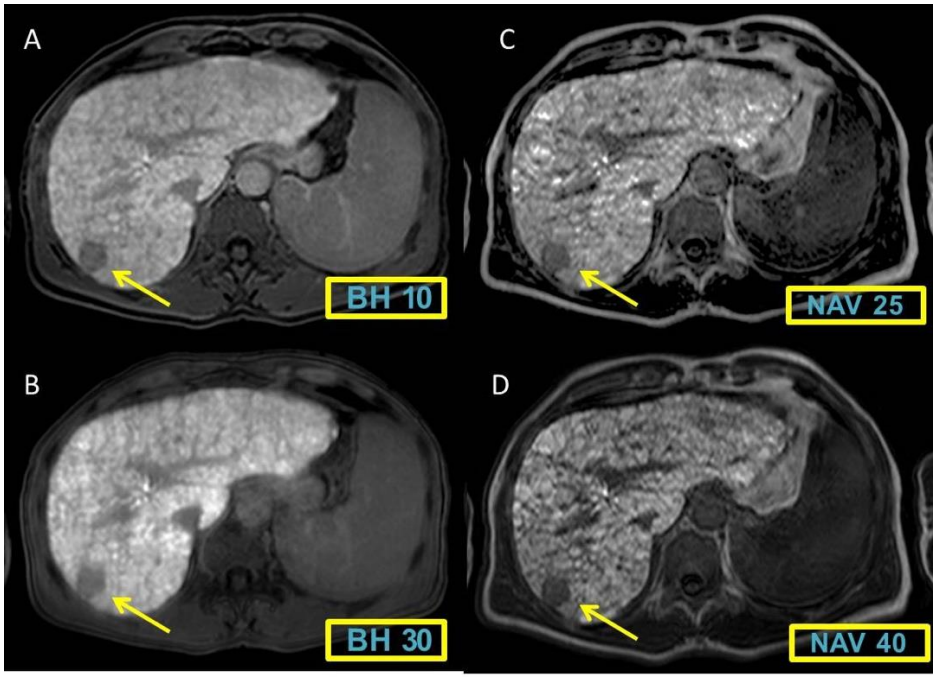

Figure 2. A 56 years-old patient with liver cirrhosis and malignant lesion (arrows). The contrast between the images is growing in Breath-hold (BH) sequences (A-B) and even greater in those with free breathing navigated sequences (NAV) (C-D).

Discussion

MR imaging with hepatospecific contrast medium, such as Gd-EOB-DTPA, though not a mandatory diagnostic tool in the EASL–EORTC and AASLD Guidelines for HCC management, was highlighted in the 2021 Consensus report from the 10th International Forum for Liver Magnetic Resonance Imaging as a particularly accurate method for diagnosing and staging HCC [14]. This technique's notable strength lies in its ability to detect hepatic nodules smaller than 1 cm, integrating hepatocytic functional analysis with a detailed vascularization profile. Such capabilities are indispensable for providing critical diagnostic insights, particularly in cases where typical imaging hallmarks of HCC are absent, allowing clinicians to spot early and potentially more treatable stages of the disease [15].

In the pathological progression of HCC nodules, affected hepatocytes undergo significant changes, primarily losing their ability to express the Organic Anion Transporter Polypeptide (OATP), crucial for transporting Gd-EOB-DTPA into healthy hepatocyte[15,16]. As this transport mechanism fails in HCC, the nodules exhibit a hypointense appearance in contrast to the surrounding healthy liver parenchyma[17,18], which intercepts approximately 50% of Gd-EOB-DTPA administered and eliminates it through bile [19–21]. The distinct difference in uptake and excretion facilitates stark contrast, pivotal for accurate lesion identification. Studies have shown that HBP imaging, when combined with dynamic phases, yelds a higher accuracy than HBP alone [22–24]. The integration of these methods has shown a sensitivity of 91.9% and a specificity of 90%, marking a significant advancement in diagnostic capabilities for liver nodules[25].

Furthermore, early-stage HCC, particularly those lacking sufficient arterial neovascularization, presents uniquely in HBP imaging as hypointense, as reported by Kim et al. This characteristic underlines the indispensable role of HBP imaging in scenarios where conventional vascular profiles used to indicate malignancy are absent. [26]. The hypointensity in HPB has been identified as a strong marker of malignancy in atypical cirrhotic nodules [22]. Additionally, longitudinal studies, like those by Sano et al, suggest that hypointense nodules in HPB may evolve into hypervascular HCC upon follow-up, indicating that loss of OATP transporters may precede arterialization, making hypointensity in HBP a potential marker of malignancy and a predictive factor [27].

 doi:10.20944/preprints202406.1104.v1

Optimized sequences, especially in HBP, are crucial for detecting suspected nodules. Unlike dynamic studies that require rapid acquisition, the contrast medium in HBP is in a pseudo-steady state, allowing for longer acquisition times in NAV sequences without being a limitation [28,29]. NAV sequences provide superior image clearness and the high spatial resolution necessary for multi-planar image reconstruction. Techniques like Maximum Intensity Projection (MIP) and minimum Intensity Projection (minIP) can distinguish small lesions from vessels [30,31].

Our findings confirm that NAV sequences offer greater diagnostic reliability compared to BH ones, particularly in terms of the radiologist's confidence in detecting lesions. Additionally, BH sequences, especially those with FA of 30° and 40°, tended to have more due to the prolonged acquisition times and to the need for extended apnoea. This underscores the advantage of free-breath sequences, which are especially beneficial for poor cooperative patients, those who can only sustain short breath-holds, children, and sedated patients [32], resulting in significantly fewer artifacts (respiratory ghosting, aliasing, zebra artifact, shading, pixel granularity). Our results demonstrate an almost complete absence of artifacts with the exception of NAV sequences with FA of 40° in which small artifacts were perceivable.

Kühn et al. observed that while post-contrast image signal intensity in liver parenchyma increases with FA, saturation artifacts worsen with higher NAV FA[33]. Our study aimed to determine the optimal FA for volumetric T1-weighted free-breathing sequences during HBP by comparing FA values up to 40°. The results, aligned with those from Nagle et all., indicated that sequences with an FA of 40° provide superior diagnostic quality, particularly those high-resolution NAV [30]. NAV sequences exhibited higher image contrast (measured as signal-to-noise ratio between liver and spleen, and liver and hypointense lesions) with the ratio increasing progressively with FA, achieving maximum results at 40°.

A technical limitation of our study was that NAV sequences were acquired after BH sequences, potentially leading to variations in lesion conspicuity due to different acquisition times and delayed excretion times, especially relevant in a population with dysfunctional livers.

This is critical for surgical planning as accurate lesion mapping can significantly influence the strategy for resection or transplantation, with direct implications on patient outcomes and the potential for complete tumor removal [5,12,13]. As surgical techniques evolve, particularly with the integration of robotic and laparoscopic approaches, the precision of preoperative imaging becomes even more crucial, underscoring the importance of continued advancements in MRI technology [5,12,13].

By enhancing the resolution and accuracy of hepatobiliary phase imaging, we can directly impact surgical approaches to liver resection and transplantation, optimizing patient outcomes and surgical precision in the management of HCC. This synergy between advanced imaging techniques and surgical innovation is key to improving the prognosis and treatment strategies for patients with hepatocellular carcinoma.

Conclusion

The findings from our study highlight the diagnostic superiority of NAV sequences over traditional BH ones in terms of image quality and relative enhancement, particularly during delayed HBP imaging with Gd-EOB-DTPA. Enhance image quality in this phase, combined with information from standard sequences, significantly boosts the radiologist's confidence in formulating a diagnosis. Thus, for clinical applications, NAV sequences should be the preferred choice over BH ones, irrespective of the radiologist's level of experience. Specifically, sequences with 40° FA during the HBP are recommended for inclusion in MRI protocols aimed at to identifing small HCC nodules. These sequences are especially beneficial for patients with limited BH capacity or those who are uncooperative, as they still deliver images with adequate diagnostic resolution and comprehensive anatomic coverage without significant increasing scan times.

The clinical relevance of this finding extends significantly into the surgical domain. The ability to accurately map and characterize liver lesions prior to surgical intervention is paramount. The high diagnostic quality of NAV sequences facilitates precise preoperative planning and can influence the

 doi:10.20944/preprints202406.1104.v1

surgical strategy, potentially impacting the choice between resection and transplantation. The detailed visualization of small and early-stage nodules allows surgeons to tailor their approaches, possibly opting for less invasive techniques or more precise resections, which could result in better preservation of liver function and improved patient outcomes.

Moreover, the utility of NAV sequences in patients who cannot maintain prolonged breath-holds (such as children, the elderly, or those in acute liver failure) ensures that high-quality diagnostic imaging is accessible to a broader patient demographic. This inclusivity is crucial for equitable healthcare delivery, particularly in managing a disease as complex and varied as hepatocellular carcinoma.

The integration of 40° FA NAV sequences into routine HBP MRI protocols not only enhances diagnostic accuracy but also enriches surgical planning and intervention strategies. This synergy between radiology and surgery underscores the importance of continuous technological advancements in MRI to improve overall treatment paradigms for HCC. Such collaborative efforts between imaging specialists and surgeons are essential for advancing patient care and optimizing outcomes in hepatobiliary medicine.

Institutional Review Board Statement: All procedures performed in studies involving human participants were in accordance with the institutional and national ethical standards.

Informed Consent Statement: Informed consent was obtained from all individual participants included in the study.

Conflicts of Interest: none.

References

1. Llovet JM, Kelley RK, Villanueva A, Singal AG, Pikarsky E, Roayaie S, et al. Hepatocellular carcinoma. Nat Rev Dis Primers 2021;7. https://doi.org/10.1038/s41572-020-00240-3.
2. EASL-EORTC Clinical Practice Guidelines: Management of hepatocellular carcinoma. n.d.
3. Okuda K. Early recognition of hepatocellular carcinoma. Hepatology 1986;6:729–38. https://doi.org/10.1002/hep.1840060432.
4. Bruix J, Sherman M. Management of hepatocellular carcinoma: An update. Hepatology 2011;53:1020–2. https://doi.org/10.1002/hep.24199.
5. Pace C, Nardone V, Roma S, Chegai F, Toti L, Manzia TM, et al. Evaluation of Contrast-Enhanced Intraoperative Ultrasound in the Detection and Management of Liver Lesions in Patients with Hepatocellular Carcinoma. J Oncol 2019;2019. https://doi.org/10.1155/2019/6089340.
6. Kudo M, Matsui O, Izumi N, Iijima H, Kadoya M, Imai Y, et al. JSH consensus-based clinical practice guidelines for the management of hepatocellular carcinoma: 2014 Update by the liver cancer study group of Japan. Liver Cancer 2014;3:458–68. https://doi.org/10.1159/000343875.
7. Tamada T, Ito K, Yamamoto A, Yasokawa K, Higaki A, Kanki A, et al. Hypointense hepatocellular nodules on hepatobiliary phase of Gd-EOB-DTPA-enhanced MRI: Can increasing the flip angle improve conspicuity of lesions? Journal of Magnetic Resonance Imaging 2013;37:1093–9. https://doi.org/10.1002/jmri.23903.
8. Sheng R, Palm V, Mayer P, Mokry T, Berger AK, Weiss KH, et al. Gadoxetic Acid-Enhanced -Phase Magnetic Resonance Imaging for Delineation of Focal Nodular Hyperplasia: Superiority of High-Flip-Angle Imaging. J Comput Assist Tomogr 2018;42:667–74. https://doi.org/10.1097/RCT.0000000000000777.
9. Gupta RT, Iseman CM, Leyendecker JR, Shyknevsky I, Merkle EM, Taouli B. Diagnosis of focal nodular hyperplasia with MRI: Multicenter retrospective study comparing gadobenate dimeglumine to gadoxetate disodium. American Journal of Roentgenology 2012;199:35–43. https://doi.org/10.2214/AJR.11.7757.
10. Haradome H, Grazioli L, Al Manea K, Tsunoo M, Motosugi U, Kwee TC, et al. Gadoxetic acid disodium-enhanced hepatocyte phase MRI: Can increasing the flip angle improve focal liver lesion detection? Journal of Magnetic Resonance Imaging 2012;35:132–9. https://doi.org/10.1002/jmri.22805.
11. Cho ES, Yu JS, Park AY, Woo ST, Kim JH, Chung JJ. Feasibility of 5-minute delayed transition phase imaging with 30° flip angle in gadoxetic acid-enhanced 3D gradient-echo MRI of liver, compared with 20-minute delayed hepatocyte phase MRI with standard 10° flip angle. American Journal of Roentgenology 2015;204:69–75. https://doi.org/10.2214/AJR.13.11903.
12. Pravisani R, De Martino M, Mocchegiani F, Melandro F, Patrono D, Lauterio A, et al. Recipient hepatectomy technique may affect oncological outcomes of liver transplantation for hepatocellular carcinoma. Liver Transpl 2024. https://doi.org/10.1097/LVT.0000000000000373.

 doi:10.20944/preprints202406.1104.v1

13. Shalaby S, Taborelli M, Zanetto A, Ferrarese A, D'Arcangelo F, Gambato M, et al. Hepatocellular carcinoma and the risk of de novo malignancies after liver transplantation – a multicenter cohort study. Transplant International 2021;34:743–53. https://doi.org/10.1111/tri.13831.
14. Taouli B, Ba-Ssalamah A, Chapiro J, Chhatwal J, Fowler K, Kang TW, et al. Consensus report from the 10th Global Forum for Liver Magnetic Resonance Imaging: developments in HCC management. Eur Radiol 2023;33:9152–66. https://doi.org/10.1007/s00330-023-09928-y.
15. Choi JY, Lee JM, Sirlin CB. CT and MR imaging diagnosis and staging of hepatocellular carcinoma. Part II. Extracellular agents, hepatobiliary agents, and ancillary imaging features. Radiology 2014;273:30–50. https://doi.org/10.1148/radiol.14132362.
16. Narita M, Hatano E, Arizono S, Miyagawa-Hayashino A, Isoda H, Kitamura K, et al. Expression of OATP1B3 determines uptake of Gd-EOB-DTPA in hepatocellular carcinoma. J Gastroenterol 2009;44:793–8. https://doi.org/10.1007/s00535-009-0056-4.
17. Kim TK, Lee KH, Jang H-J, Haider MA, Jacks LM, Menezes RJ, et al. Analysis of Gadobenate Dimeglumine-enhanced MR Findings for Characterizing Small (1-2-cm) Hepatic Nodules in Patients at High Risk for Hepatocellular Carcinoma 1 From the Departments of Medical Imaging (T 2011;259. https://doi.org/10.1148/radiol.11101549/-/DC1.
18. Ahn SJ, Shin HJ, Chang JH, Lee SK. Differentiation between primary cerebral lymphoma and glioblastoma using the apparent diffusion coefficient: Comparison of three different ROI methods. PLoS One 2014;9. https://doi.org/10.1371/journal.pone.0112948.
19. Spinazzi A, Lorusso V, Pirovano G, Taroni P, Kirchin M, Davies A. MultiHance Clinical Pharmacology: Biodistribution and MR Enhancement of the Liver 1. n.d.
20. Hamm B, Staks T, M#{252}hler A, Bolbow M, Taupitz M, Frenzel T, et al. Phase I Clinical Evaluation of Gd-EOB-DTPA as a Hepatobiliary MR Contrast Agent: Safety, Pharmacokinetics, and MR Imaging'. n.d.
21. Park Y, Kim SH, Kim SH, Jeon YH, Lee J, Kim MJ, et al. Gadoxetic acid (Gd-EOB-DTPA)-enhanced mri versus gadobenate dimeglumine (Gd-BOPTA)-enhanced MRI for preoperatively detecting hepatocellular carcinoma: An initial experience. Korean J Radiol 2010;11:433–40. https://doi.org/10.3348/kjr.2010.11.4.433.
22. Golfieri R, Grazioli L, Orlando E, Dormi A, Lucidi V, Corcioni B, et al. Which is the best MRI marker of malignancy for atypical cirrhotic nodules: Hypointensity in hepatobiliary phase alone or combined with other features? Classification after Gd-EOB-DTPA administration. Journal of Magnetic Resonance Imaging 2012;36:648–57. https://doi.org/10.1002/jmri.23685.
23. Tsuboyama T, Onishi H, Kim T, Akita H, Hori M, Tatsumi M, et al. Hepatocellular carcinoma: Hepatocyte-selective enhancement at gadoxetic acid-enhanced MR imaging - Correlation with expression of sinusoidal and canalicular transporters and bile accumulation. Radiology 2010;255:824–33. https://doi.org/10.1148/radiol.10091557.
24. Onishi H, Kim T, Imai Y, Hori M, Nagano H, Nakaya Y, et al. Hypervascular hepatocellular carcinomas: Detection with gadoxetate disodium-enhanced MR imaging and multiphasic multidetector CT. Eur Radiol 2012;22:845–54. https://doi.org/10.1007/s00330-011-2316-y.
25. Orlacchio A, Chegai F, Fabiano S, Merolla S, Funel V, Di Giuliano F, et al. Role of MRI with hepatospecific contrast agent in the identification and characterization of focal liver lesions: pathological correlation in explanted livers. Radiologia Medica 2016;121:588–96. https://doi.org/10.1007/s11547-016-0636-3.
26. Kim YK, Lee WJ, Park MJ, Kim SH, Rhim H, Choi D. Hypovascular hypointense nodules on hepatobiliary phase gadoxetic acid-enhanced MR images in patients with cirrhosis: Potential of DW imaging in predicting progression to hypervascular HCC. Radiology 2012;265:104–14. https://doi.org/10.1148/radiol.12112649.
27. Sano K, Ichikawa T, Motosugi U, Ichikawa S, Morisaka H, Enomoto N, et al. Outcome of hypovascular hepatic nodules with positive uptake of gadoxetic acid in patients with cirrhosis. Eur Radiol 2017;27:518–25. https://doi.org/10.1007/s00330-016-4423-2.
28. Yoon JH, Lee JM, Lee ES, Baek J, Lee S, Iwadate Y, et al. Navigated three-dimensional T1-weighted gradient-echo sequence for gadoxetic acid liver magnetic resonance imaging in patients with limited breath-holding capacity. Abdom Imaging 2015;40:278–88. https://doi.org/10.1007/s00261-014-0214-x.
29. Lee JM, Zech CJ, Bolondi L, Jonas E, Kim MJ, Matsui O, et al. Consensus report of the 4th international forum for gadolinium-ethoxybenzyl-diethylenetriamine pentaacetic acid magnetic resonance imaging. Korean J Radiol 2011;12:403–15. https://doi.org/10.3348/kjr.2011.12.4.403.
30. Nagle SK, Busse RF, Brau AC, Brittain JH, Frydrychowicz A, Iwadate Y, et al. High resolution navigated three-dimensional T1-weighted hepatobiliary MRI using gadoxetic acid optimized for 1.5 tesla. Journal of Magnetic Resonance Imaging 2012;36:890–9. https://doi.org/10.1002/jmri.23713.
31. Brismar TB, Dahlström N, Edsborg N, Persson A, Smedby Ö, Albiin N. Liver vessel enhancement by Gd-BOPTA and Gd-EOB-DTPA: A comparison in healthy volunteers. Acta Radiol 2009;50:709–15. https://doi.org/10.1080/02841850903055603.

 doi:10.20944/preprints202406.1104.v1

32. Vasanawala SS, Iwadate Y, Church DG, Herfkens RJ, Brau AC. Navigated abdominal T1-W MRI permits free-breathing image acquisition with less motion artifact. Pediatr Radiol 2010;40:340–4. https://doi.org/10.1007/s00247-009-1502-4.
33. Küuhn JP, Holmes JH, Brau ACS, Iwadate Y, Hernando D, Reeder SB. Navigator flip angle optimization for free-breathing T1-weighted hepatobiliary phase imaging with gadoxetic acid. Journal of Magnetic Resonance Imaging 2014;40:1129–36. https://doi.org/10.1002/jmri.24480.